
Article:
Aryan, H., Agapitov, O.V., Artemyev, A. et al. (4 more authors) (2020) Outer radiation belt electron lifetime model based on combined Van Allen Probes and Cluster VLF measurements. Journal of Geophysical Research: Space Physics, 125 (8). e2020JA028018. ISSN 2169-9380

https://doi.org/10.1029/2020ja028018

JGR Space Physics

RESEARCH ARTICLE
10.1029/2020JA028018

Outer Radiation Belt Electron Lifetime Model Based on Combined Van Allen Probes and Cluster VLF Measurements

Homayon Aryan[1,2], Oleksiy V. Agapitov[3], Anton Artemyev[4], Didier Mourenas[5], Michael A. Balikhin[2], Richard Boynton[2], and Jacob Bortnik[1]

[1]Atmospheric and Oceanic Sciences, University of California Los Angeles, Los Angeles, CA, USA, [2]Department of Automatic Control and Systems Engineering, University of Sheffield, Sheffield, UK, [3]Space Sciences Laboratory, University of California Berkeley, Berkeley, CA, USA, [4]Earth, Planetary, and Space Sciences, University of California, Los Angeles, CA, USA, [5]CEA/DAM Ile de France, Arpajon, France

Key Points:
- A comprehensive parametric model of electron lifetime in the outer radiation belt has been developed
- Model lifetimes are compared with analytical results and measured data
- The model provides accurate estimates of electron lifetimes over a wide range of energies as a function of geomagnetic activity

Correspondence to:
H. Aryan,
aryan.homayon@gmail.com

Citation:
Aryan, H., Agapitov, O. V., Artemyev, A., Mourenas, D., Balikhin, M. A., & Boynton, R., et al. (2020). Outer radiation belt electron lifetime model based on combined Van Allen Probes and Cluster VLF measurements. *Journal of Geophysical Research: Space Physics*, *125*, e2020JA028018. https://doi.org/10.1029/2020JA028018

Received 17 MAR 2020
Accepted 4 JUN 2020
Accepted article online 22 JUL 2020

Abstract The flux of energetic electrons in the outer radiation belt shows a high variability. The interactions of electrons with very low frequency (VLF) chorus waves play a significant role in controlling the flux variation of these particles. Quantifying the effects of these interactions is crucially important for accurately modeling the global dynamics of the outer radiation belt and to provide a comprehensive description of electron flux variations over a wide energy range (from the source population of 30 keV electrons up to the relativistic core population of the outer radiation belt). Here, we use a synthetic chorus wave model based on a combined database compiled from the Van Allen Probes and Cluster spacecraft VLF measurements to develop a comprehensive parametric model of electron lifetimes as a function of L-shell, electron energy, and geomagnetic activity. The wave model takes into account the wave amplitude dependence on geomagnetic latitude, wave normal angle distribution, and variations of wave frequency with latitude. We provide general analytical formulas to estimate electron lifetimes as a function of L-shell (for $L = 3.0$ to $L = 6.5$), electron energy (from 30 keV to 2 MeV), and geomagnetic activity parameterized by the *AE* index. The present model lifetimes are compared to previous studies and analytical results and also show a good agreement with measured lifetimes of 30 to 300 keV electrons at geosynchronous orbit.

Plain Language Summary The space surrounding our planet is full of charged particles trapped in donut-shaped belts called the Van Allen radiation belts that encircle the Earth. These charged particles can cause significant malfunctions and unexpected failures to spacecraft electronics. The intensity of the radiation belts vary as these energetic particles interact with very low frequency (VLF) waves such as chorus waves. Therefore, it is crucially important to accurately quantify the wave-particle interactions for accurately modeling and forecasting the global dynamics of the Van Allen radiation belts. Predicting the magnitude and duration of potentially hazardous conditions could help satellite operators to switch off nonessential satellite electronic systems to reduce malfunctions and unexpected failures only during the most dangerous periods. In this study, we use a chorus wave model based on multi-satellite wave measurements to calculate the lifetimes of these charged particles in the Earth's Van Allen radiation belts. We then compare our results with previous studies, analytical results, and measured data.

1. Introduction

Energetic electron fluxes in the outer radiation belt show high variability, especially during geomagnetically disturbed conditions where the fluxes of electrons can vary by several orders of magnitude (Reeves et al., 2003) over a period of an hour or less. Such extreme variations in relativistic electron fluxes can cause significant malfunctions and unexpected failures of spacecraft electronics (Horne, 2007). Wave-particle interactions with very low frequency (VLF) chorus waves play an important role in controlling the flux variation of these particles (Bortnik & Meredith, 2008; Bortnik & Thorne, 2007; Bortnik, Thorne, & Meredith 2007; Bortnik, Thorne, Meredith, & Santolik 2007; Millan & Thorne, 2007; Shprits, Elkington, et al., 2008). Chorus waves significantly contribute to the acceleration and scattering of energetic electrons into the loss cone. These waves are right-hand-polarized, intense electromagnetic whistler mode emissions with short,

relatively coherent and repetitive rising or falling tones. The most intense emissions are observed during geomagnetically active conditions and are located from premidnight to postmidday (Agapitov et al., 2013; Aryan et al., 2014, 2016, 2017; Boynton et al., 2018; Burtis & Helliwell, 1976; Li et al., 2011; Meredith et al., 2001; Santolík et al., 2004). They are observed in two distinct frequency bands: the lower band chorus 0.1–0.5f_{ce} and the upper band chorus 0.5–0.8f_{ce} with a power gap separating the bands at 0.5f_{ce} (Sazhin & Hayakawa, 1992; Tsurutani & Smith, 1974), where f_{ce} is the equatorial electron gyrofrequency. It is known that the two bands interact with different electron energy populations. The upper band chorus waves interact mainly with the lower energy electrons (<50 keV) (Ma et al., 2016), whereas the lower band parallel and oblique chorus waves can affect electrons on a much wider energy range from 0.1 keV to multi-MeVs (Artemyev et al., 2015) and contribute strongly to the quickly evolving dynamics of radiation belt electron fluxes (Artemyev et al., 2016; Horne et al., 2005; Li, Ma et al., 2016; Mourenas et al., 2014; Mourenas et al., 2016; Shprits, Subbotin et al., 2008; Thorne et al., 2013; Tu et al., 2014).

It is crucial to quantify the effects of these interactions for accurately modeling and forecasting the global dynamics of the outer radiation belt and for providing a comprehensive description of electron flux variations over a wide energy range, from the source population of ~10- to 50 keV electrons up to the relativistic core population of the outer radiation belt. This requires complete spatiotemporal coverage of the inner magnetosphere to provide comprehensive and accurate statistics of chorus waves encompassing the entire parameter space. However, it is unlikely to achieve such comprehensive coverage with a given spacecraft mission. Therefore, in this study, we use a synthetic empirical wave model, developed by Agapitov et al. (2018) based on combined VLF measurements from the Van Allen Probes and Cluster spacecraft, to develop a comprehensive parametric model of electron lifetimes in the outer radiation belt as a function of geomagnetic activity (AE), L-shell (L), electron energy (E), and magnetic local time (MLT). The wave model takes into account the wave amplitude dependence on geomagnetic latitude, wave normal angle distribution, and variations of wave frequency with latitude. The resulting synthetic statistical model of chorus wave amplitude, obliquity, and frequency is presented in the polynomial form of geomagnetic activity level in three MLT sectors, L-shell, and for a range of electron energies. In the next section we describe the synthetic chorus wave model in detail and how we use the model to calculate electron lifetimes in the outer radiation belt. We then describe and discuss the results and compare them with analytical results and measured data.

2. Synthetic Chorus Wave Model

The synthetic model describing chorus waves amplitudes and the wave normal angle distribution (Agapitov et al., 2015, 2018) has been previously derived from the combined statistics of the Van Allen Probes and Cluster satellites VLF measurements. The combined chorus data set includes more than 5 years of Van Allen Probes and 10 years of Cluster VLF measurements. The Van Allen Probes provide excellent coverage of relatively low L-shells and low latitudes, but the coverage becomes more sparse at high latitudes and terminates at $L > 6$. In contrast, the Cluster spacecraft provide good coverage of high-latitude (up to $\lambda = 45°$) and high-L ($L > 6$) regions, but limited coverage of the low latitudes, especially in the night sector. Hence, the combination of the two data sets provides complementary coverage of geomagnetic latitudes up to 45° in the chorus frequency range 0.1f_{ce} to 0.8f_{ce}. The database of VLF wave measurements includes the wave amplitude dependence on geomagnetic latitude, wave normal angle distribution, and variations of wave frequency with latitude.

The resulting synthetic model of chorus waves properties includes fits for the wave amplitude, wave frequency, and wave normal angle distribution as a function of magnetic latitude (λ), MLT, and L above the plasmapause. The synthetic chorus model provides the wave amplitude distribution from the equator up to $\lambda = 45°$ for $Kp = 0$–6 and $L \approx 4$–7. For the purpose of this study, we have modified the model to consider three ranges of AE index. The AE index is one of the most influential parameters that define chorus wave activity (Aryan et al., 2014; Boynton et al., 2018; Zhang et al., 2018). The average amplitude of chorus waves can be well parameterized by AE, which provides a measure of injections and convection of energetic electrons that generate such waves (Li et al., 2011; Meredith et al., 2001; Shprits et al., 2007). Therefore, the present study paves the way for developing a future multiparameter wave model that will also include solar wind parameters (Aryan et al., 2014, 2017). An approximately dipolar geomagnetic field and McIlwain L-shells are considered in the chorus model (Agapitov et al., 2015, 2018). This dipolar field model can

become inaccurate at $L > 5$ during magnetic storms or strong substorms with $AE > 200$–300 nT. Therefore, to mitigate the potential impact of errors in L-shells on the chorus model, two relatively wide L-shell bins are considered, extending from the plasmapause ($L \sim 3$–4) to $L = 5$, and from $L = 5$ to $L = 7$, respectively (Agapitov et al., 2015, 2018). In addition, there is presently no magnetic field model that accurately incorporates substorm effects through the *AE* index, and all existing disturbed field models differ significantly from each other (Huang et al., 2008; Lu et al., 1999). The chorus wave model dependence of wave amplitude *Bw* on λ is presented in Figure 1, and the corresponding tables of coefficients of the model fits can be found in Agapitov et al. (2018). The wave normal angular distribution of lower band chorus is presented as a combination of field-aligned wave normal angle population with Gaussian distribution around the background magnetic field direction and the population of oblique waves with Gaussian distribution in the wave normal range between the local Gendrin angle and the resonance cone as presented in Equation 1 (Agapitov et al., 2015, 2018):

$$g(\theta) = exp\left(-\frac{(\theta-\theta_1)^2}{\delta\theta_1^2}\right) + Q^2 exp\left(-\frac{(\theta-\theta_2)^2}{\delta\theta_2^2}\right) \quad (1)$$

where the factor Q depends on L, λ, MLT, and geomagnetic activity with the approximation from Agapitov et al. (2018) (presented in Figure 1), θ_1 and θ_2, $\delta\theta_1 \approx \delta\theta_2 \approx 8°$ were determined by Agapitov et al. (2015) and can be approximated by polynomials on λ:$\theta_1 = 11.5 + 14.3\lambda/10 - 8.1(\lambda/10)^2 + 1.2(\lambda/10)^3$ and $\theta_2 = 66 + 0.1(\lambda/10)$. The model takes into account the significant population of very oblique waves recorded in the night/morning sector by the Van Allen Probes at low latitudes during disturbed periods (Agapitov et al., 2014, 2016; Li et al., 2016). The chorus mean frequency depends on λ (as reported earlier by Breuillard et al., 2012, 2015, and Bunch et al., 2013) that is represented in Agapitov et al. (2018) by the linear dependence of the mean frequency f_m: $f_m/f_{ce} = 0.35 - 0.0125\lambda$ with a variance of 0.07. This frequency dependence decreases the latitude of cyclotron resonances and (as *Bw* goes down with λ) increases 2–5 times the effective wave amplitude (Agapitov et al., 2018).

3. Electron Lifetimes

Electron decay time constants (i.e., lifetime) estimates are very useful for radiation belt modeling, for instance, to accurately incorporate electron loss in radial diffusion models with a loss term (Schulz & Lanzerotti, 1974). In this study, the synthetic chorus wave model described in the previous section is used to calculate the local pitch angle diffusion coefficients ($D_{\alpha\alpha}$) for electrons over a wide energy range (1 keV to 2 MeV), as a function of geomagnetic activity, L, and MLT. Figure 2 shows the local bounce-averaged pitch angle diffusion coefficients ($D_{\alpha\alpha}$) at $L = 4$ for quiet (left: $AE < 100$ nT), moderate (middle: $100 \leq AE \leq 300$ nT), and active (right: $AE > 300$ nT) geomagnetic conditions as a function of electron energy and equatorial pitch angle (α_{eq}°). The $D_{\alpha\alpha}$ values are shown for night (row 1: MLT > 21 and MLT ≤ 03), dawn (row 2: 03 < MLT ≤ 09), day (row 3: 09 < MLT ≤ 15), and averaged MLT. Overall, the electron scattering rates are low during quiet conditions but significantly increase during moderate and active geomagnetic conditions, especially for low-energy electrons (<100 keV). For moderate and high geomagnetic activities, a significant scattering is observed for electrons with low energies (less than ~100 keV) and small pitch angles, which are rapidly precipitated into the atmosphere. However, for quiet geomagnetic conditions, the scattering rates appear relatively weak, and the highest electron scattering rates are observed for electrons with energies in the range of approximately 10–1,000 keV and are enhanced during moderate and high geomagnetic activities. Also, the scattering rates vary noticeably across MLT. Dawn and night sector scattering is generally stronger than dayside scattering, especially for low-energy <100 keV electrons or for high energy >100 keV electrons with high pitch angles, due to the more intense chorus wave activity near the equator (where these electrons reach cyclotron resonance with the waves) on the dawn/night sector compared to day sector. The MLT-averaged diffusion rates have similar features of intense scattering as on the dawn side.

We studied the local pitch angle diffusion coefficients for a range of L-shell from $L = 3.0$ to $L = 6.5$. Figure 3 shows the MLT-averaged pitch angle diffusion coefficients ($D_{\alpha\alpha}$) at $L = 3.0$–6.5 (top to bottom) for quiet (left), moderate (middle), and active (right) geomagnetic conditions as a function of electron energy and equatorial pitch angle (α_{eq}°). In general, the rate of electron scattering depicts a similar trend across all

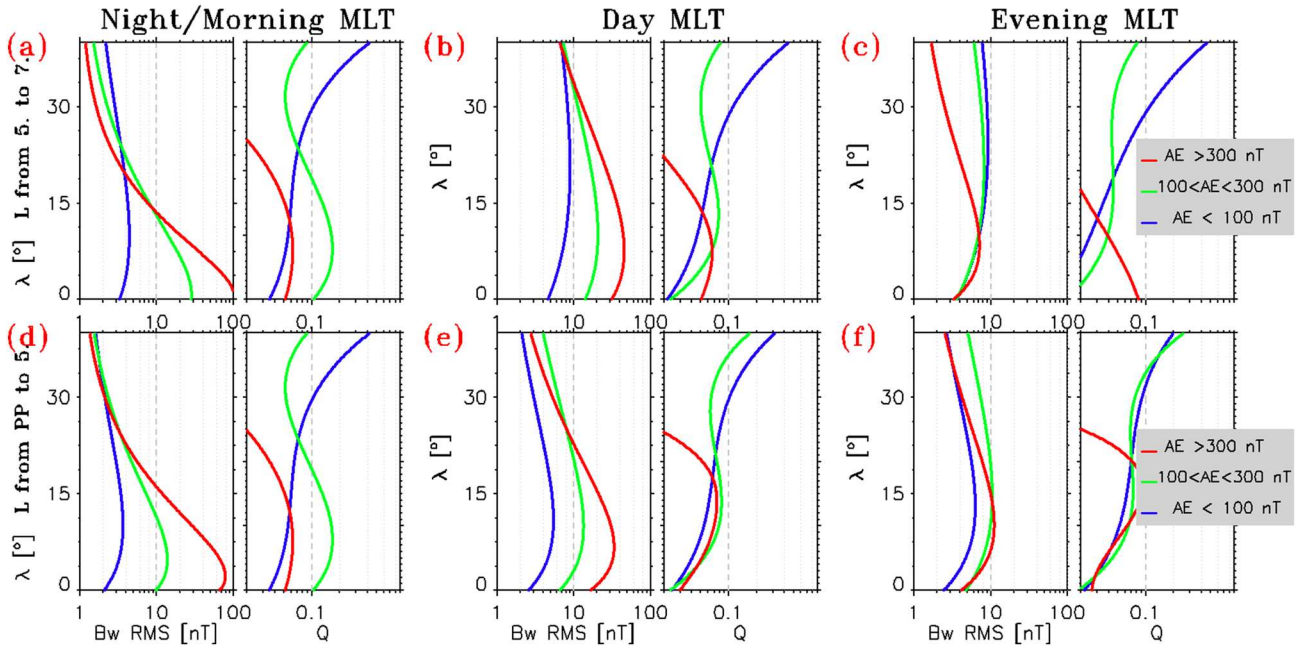

Figure 1. Chorus RMS (root mean square) amplitudes (left) and wave normal angle obliqueness parameter Q (right) for L-shell ranges from 5 to 7 (a–c) and from the plasmapause to $L = 5$ (d–f) in the night/morning, day, and evening MLT sectors.

L-shells (weak scattering during quiet conditions, but intense scattering during moderate and active geomagnetic conditions for low-energy electrons with energies of approximately less than 100 keV). However, there is an increase in the rate of electron scattering at higher L-shells, for all geomagnetic conditions, where chorus wave activity is more intense. The scattering rates can vary by up to an order of a magnitude in MLT, especially, for electrons with energies of ~10–1,000 keV during quiet conditions. Nevertheless, as we are interested in calculating electron lifetimes over hours to days, and since >30 keV electrons drift azimuthally around the Earth in less than 1 hr at $L > 4$, it is justified to consider the MLT-averaged diffusion rates actually experienced by such electrons. Such MLT-averaged diffusion rates have been checked in past works to accurately provide equilibrium electron loss rates following storms (Shprits et al., 2009).

The lifetimes of electrons are calculated by integrating $1/[4 * tan(\alpha_{eq}) * D_{\alpha\alpha}]$ from small $\alpha_{eq} = \alpha_{LC}$ (at the loss cone) up to $\alpha_{eq} \approx 60°$ and for the MLT-averaged $D_{\alpha\alpha}$ larger than 10^{-8}) (Albert & Shprits, 2009; Artemyev et al., 2013; Mourenas et al., 2012). Figure 4 shows electron lifetimes as a function of L and electron energy for quiet (left), moderate (middle), and active (right) geomagnetic conditions. During quiet conditions, electron lifetimes are relatively long, >10 days, for a wide range of electron energies. However, the lifetimes become shorter during moderate and active geomagnetic conditions, especially, for low-energy electrons (<100 keV) that can be quickly (in less than 1–3 hr) precipitated into the atmosphere by chorus waves. This strong reduction of low-energy electron lifetimes is mainly due to the increase of MLT-averaged magnetic chorus wave power with *AE* at low latitudes <20° (see Figure 2), where such electrons reach cyclotron resonance with quasi-parallel waves. In fact, the ~10- to 50 keV electron population provides the free energy source for chorus waves generation (see Figure 1 from Agapitov et al., 2018).

Various studies have noted the importance of electron loss due to resonant chorus wave-particle interactions (Albert & Shprits, 2009; Shprits, Elkington et al., 2008; Thorne, 2010). The present results are comparable with previous studies, in particular with the results from Orlova and Shprits (2014) who provided realistic lifetime models based on previous, more limited statistics of chorus wave amplitude distributions. However, we have developed a comprehensive parametric model of electron lifetimes based on comprehensive coverage of VLF measurements provided by multiple spacecraft. Here we compare the results of the present model of electron lifetimes with analytical lifetime estimates provided by Mourenas et al. (2014) and with actual lifetimes measured at geosynchronous orbit (GEO) (Boynton et al., 2014).

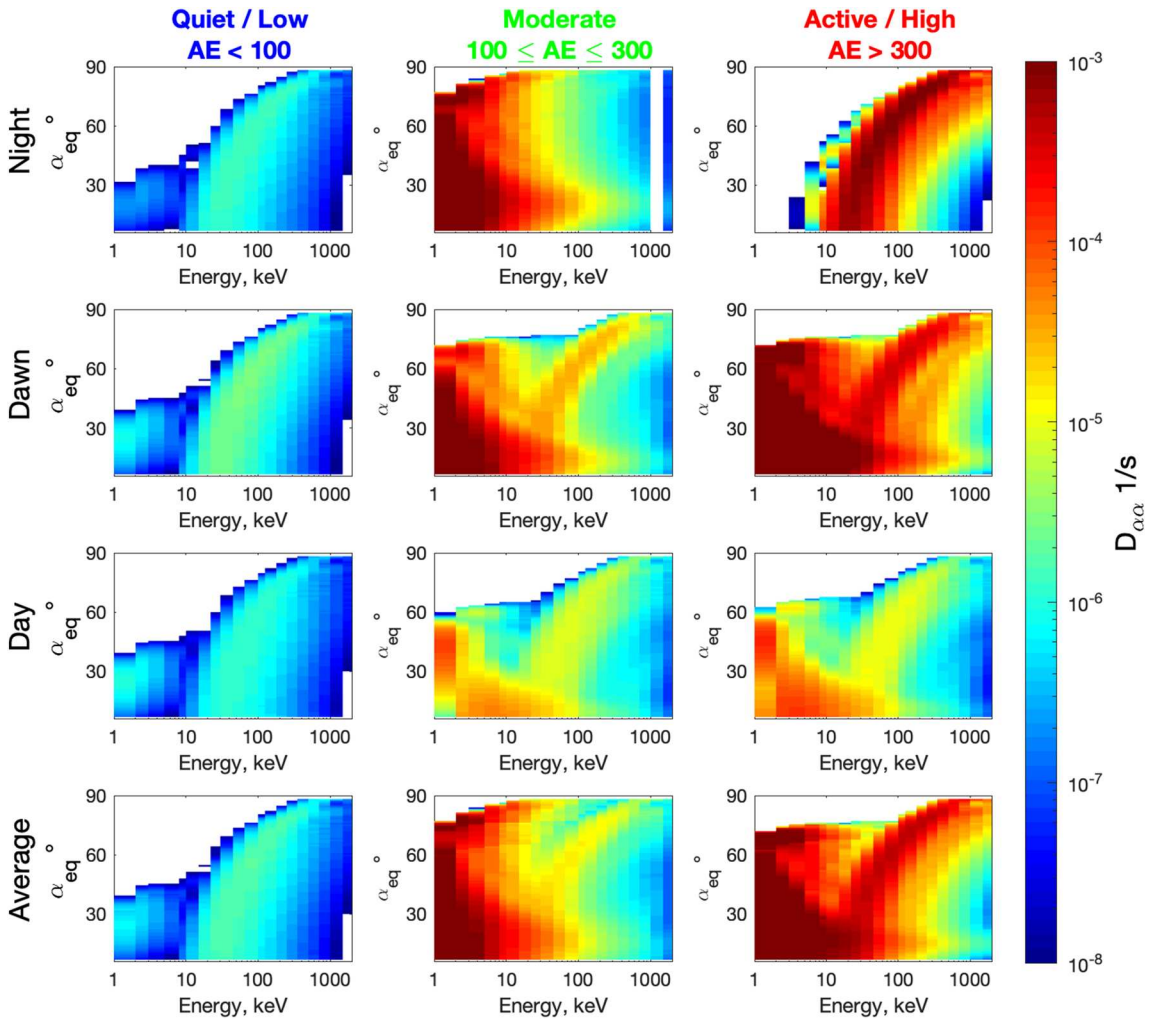

Figure 2. The local pitch angle diffusion coefficients ($D_{\alpha\alpha}$) at $L = 4$ for quiet (left), moderate (middle), and active (right) geomagnetic conditions as a function of electron energy and equatorial pitch angle (αeq). The $D_{\alpha\alpha}$ values are shown for night (row 1: MLT > 21 and MLT ≤ 03), dawn (row 2: 03 < MLT ≤ 09), day (row 3: 09 < MLT ≤ 15), and averaged over MLT.

Mourenas et al. (2014) derived two approximate analytical lifetime estimates, by considering either only quasi-parallel chorus waves as in observations at latitudes >10° during active periods or a reasonable proportion of very oblique chorus waves together with a main population of quasi-parallel waves as in observations during weakly disturbed geomagnetic conditions (see Figure 1 here; see also Mourenas et al., 2014; Agapitov et al., 2018). Here, we shall consider for simplicity the expression derived for quasi-parallel waves (Mourenas et al., 2014), valid for $E[\mathrm{keV}] > 30(6.6/L)^2$ (for cyclotron resonance to be available), assuming a plasma density variation given by the statistical model of Sheeley et al. (2001).

$$\tau[\mathrm{days}] = \frac{200[\mathrm{days\ pT^2}](E[\mathrm{keV}]/511+1)\left((E[\mathrm{keV}]/511+1)^2-1\right)^{3/4}}{\left(Bw[\mathrm{pT}](L/6.6)^{3/4}\right)^2} \quad (2)$$

At $L = 6.6$ (i.e., Geosynchronous Earth Orbit), we use MLT-averaged and latitude-averaged (over 10–30°) chorus wave amplitudes $Bw = 6$ and 12 pT during quiet and moderately disturbed geomagnetic conditions, respectively, in rough agreement with Figures 1a–1c results. During active periods, however, the wave amplitude decreases significantly at higher latitudes. In addition, we should consider the wave amplitude Bw at the latitude of cyclotron resonance, that is, near 13° for 30 keV, 18° for 100 keV, and 30° for 1 MeV (e.g., see Figure 2 from Agapitov et al., 2018). Note that the decrease of the wave mean frequency toward

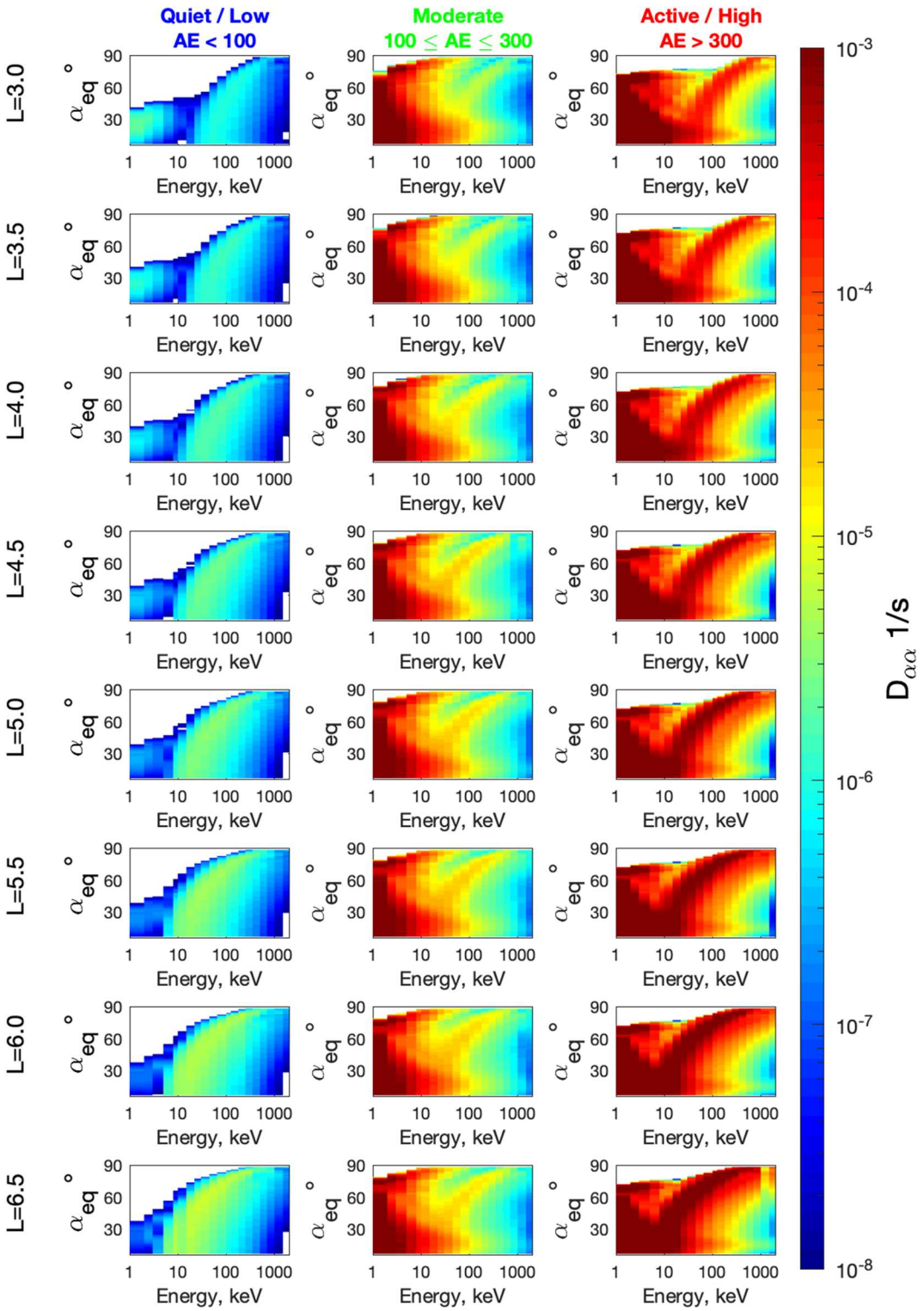

Figure 3. The average pitch angle diffusion coefficients ($D_{\alpha\alpha}$) at $L = 3.0$–6.5 (top to bottom at $L = 0.5$ intervals) for quiet (left), moderate (middle), and active (right) geomagnetic conditions as a function of electron energy and equatorial pitch angle (αeq).

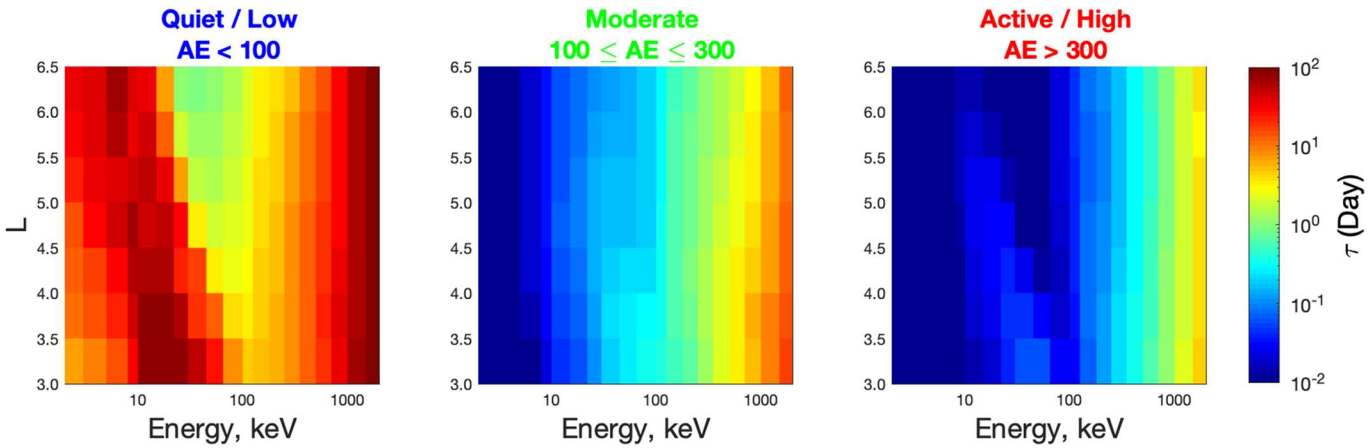

Figure 4. Electron lifetimes as a function of L and electron energy for quiet (left), moderate (middle), and active (right) geomagnetic conditions.

higher latitudes in our chorus model leads to a decrease of the latitude of electron cyclotron resonance with the waves, as compared with the case of a constant mean frequency $\sim 0.35 f_{ce}$, and it gives also a slightly faster decrease of this latitude of cyclotron resonance from high to low electron energy (Agapitov et al., 2018). All this leads us to take approximately $Bw = (30\,\text{pT}) * 1/(1+E[\text{keV}]/511)^{1/2}$ during active periods. Figure 5a shows electron lifetimes as a function of electron energy, allowing us to compare the results of the present full numerical model (solid curves) with the above analytical lifetime estimates (dashed curves) valid only for $E > 30(6.6/L)^2$ keV—that is for electron diffusion through cyclotron resonance with the waves (Mourenas et al., 2012, 2014). The present model results are in rough agreement with the analytical estimates over many decades. In particular, the model lifetimes follow approximately the same analytical scaling with energy given by Equation 2, except at low energies <70 keV during periods of elevated AE activity. This discrepancy at low energies for high AE is due to the steep peak of wave power present at low latitudes (where cyclotron resonance occurs at low energies) in the night/dawn sector when $AE > 300$ nT (see Figure 1d), which is not fully taken into account in the above analytical estimates. For a constant chorus wave amplitude Bw (that would not decrease with latitude), both the analytical and full numerical lifetimes would increase less rapidly with energy in Figure 5a, especially during moderate to

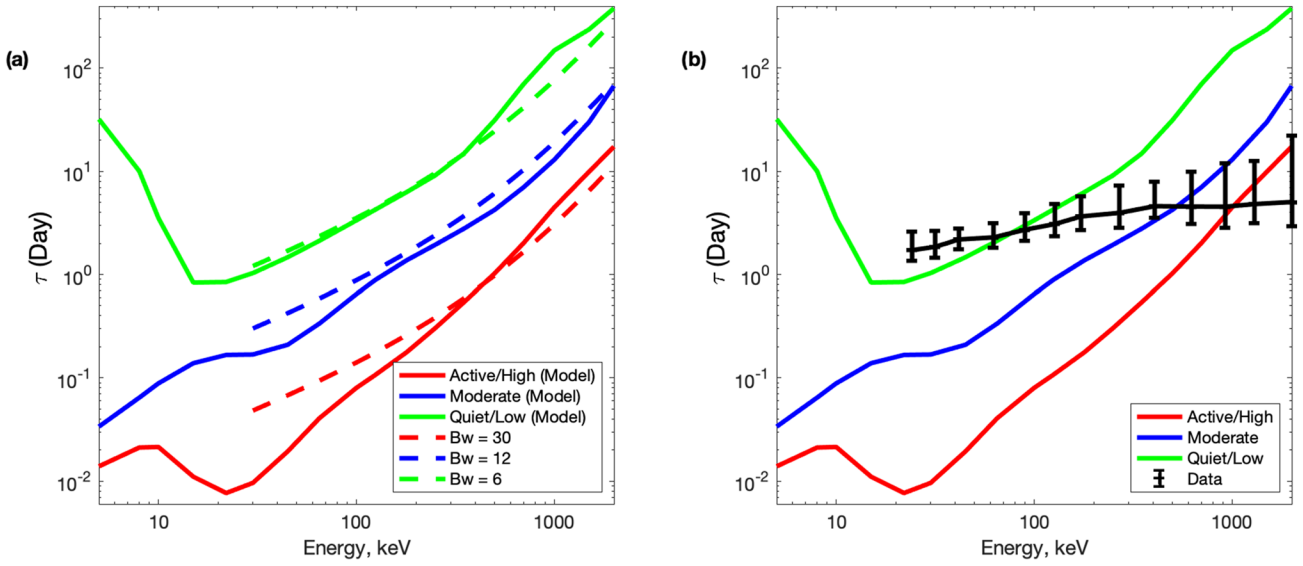

Figure 5. Electron lifetimes as a function of electron energy: (a) numerical model (solid curves) at $L = 6.5$ and analytical lifetime estimates (dashed curves) at $L = 6.5$. (b) Numerical model as presented in panel (a) and the measured average electron lifetimes at $L \sim 6.6$, GEO (black curve) (Boynton et al., 2014), together with 10th and 90th percentiles.

Table 1
The Average Bw (pT) That Provides the Best Agreement Between Analytical and Model Lifetimes as a Function of E and L for Quiet (AE < 100 nT), Moderate (100 ≤ AE ≤ 300 nT), and Active (AE > 300 nT) Geomagnetic Conditions

L	Bw (AE <100 nT)	Bw (100 ≤ AE ≤ 300 nT)	Bw (AE > 300 nT)
3.0	7.8	23.5	57.6
3.5	7.2	20.7	54.7
4.0	6.8	19.5	52.2
4.5	6.5	18.8	49.0
5.0	6.3	17.9	45.7
5.5	6.1	17.4	42.9
6.0	6.0	16.6	39.0
6.5	5.8	14.5	37.2
E (keV)	Bw (AE < 100 nT)	Bw (100 ≤ AE ≤ 300 nT)	Bw (AE > 300 nT)
30	5.2	20.1	70.8
45	6.4	20.4	71.3
65	7.0	20.9	63.1
100	7.1	19.1	53.6
125	7.1	18.2	50.4
180	7.2	17.4	46.6
250	7.0	17.4	43.8
350	6.9	17.8	41.0
500	6.6	18.4	38.3
700	6.1	18.4	35.6
1,000	5.5	18.6	33.4
1,500	6.3	18.0	32.6
2,000	6.6	16.4	32.3

high AE periods, characterized by a faster increase of lifetimes with energy due to the faster decrease of Bw with latitude.

Figure 5b allows us to compare the model results with the measured average electron lifetimes at $L = 6.6$ (Boynton et al., 2014), together with 10th and 90th percentiles. The model lifetimes, corresponding to quiet periods, agree well with measured lifetimes for moderate energy (<300 keV) electrons. At higher energies (>300 keV), the measured lifetimes become smaller than model lifetimes during low AE activity (green solid line), falling in closer agreement with model lifetimes for moderate activity ($100 < AE < 300$ nT). This behavior is probably partly due to the upper limit of <20 days imposed on measured lifetimes by the method of empirical lifetime determination, in the presence of low measured fluxes at high E (Boynton et al., 2014). Possible physical causes of discrepancies between estimated and measured lifetimes will be discussed in the next section.

As shown in Figure 5a the model lifetimes at GEO follow approximately the same analytical scaling with energy given by Equation 2. Here we refine and generalize Equation 2, deriving analytical lifetime fits to the full model lifetimes as a function of energy and L-shell in the range of $30 \le E \le 2{,}000$ keV and $3 \le L \le 6.5$, respectively. We use the analytical formula in Equation 2 to find numerically the polynomial function $Bw(L, E)$ that provides the best agreement at all (E, L) with model lifetimes. Table 1 shows the average Bw that provides the best agreement between analytical and model lifetimes as a function of E and L for quiet ($AE < 100$ nT), moderate ($100 \le AE \le 300$ nT), and active ($AE > 300$ nT) geomagnetic conditions. In general, for quiet and moderate geomagnetic conditions the average Bw does not change significantly with E. Therefore, for quiet and moderate geomagnetic conditions we simply drive polynomial fits for Bw as a function of L given by Equations 3 and 4, respectively.

$$Bw(L,\ \text{quiet}) = -0.5L + 9.1\ \text{pT} \tag{3}$$

$$Bw(L,\ \text{moderate}) = -2.2L + 28.9\ \text{pT} \tag{4}$$

For active geomagnetic conditions, however, Bw clearly changes significantly with E and L, due to the faster latitudinal decrease of Bw. In this case, for the average L we derive the best polynomial fit in the form of $Bw(E) = Bw(30\ \text{keV})$ * Exp(X^(Y/ E[keV])), where X and Y values are determined by minimizing the maximum value of Log([lifetime fit/full numerical lifetime] − 1). This is an unbiased and symmetric minimization, roughly equivalent to minimizing the median symmetric accuracy from Morley et al. (2018). The best values for X and Y are calculated as $X = -0.1$ and $Y = 74$. To account for the variation of Bw for different L-shells, we write the polynomial in the form of $Bw(E,L) = Bw(30\ \text{keV})$ * Exp(−0.1^(74/ E[keV])) + Z($L - L$) and calculate the value of Z, $Z = -6$, (where $L = 4.75$, is the mean value of L considered in this study). Therefore, the full polynomial for active geomagnetic conditions is given by Equation 5:

$$Bw(L,\ E,\ \text{high}) = Bw(30\ keV) * Exp(-0.1\ \hat{}\ (74/E[\text{keV}])) - 6(L - L)\ \text{pT} \tag{5}$$

The polynomial functions presented in Equations 3–5 are substituted into Equation 2 to provide general analytical formulas given by Equations 6–8:

$$\tau[\text{days},\ \text{quiet}] = \frac{200[\text{days pT}^2](E[\text{keV}]/511 + 1)\left((E[\text{keV}]/511 + 1)^2 - 1\right)^{3/4}}{\left((-0.5L + 9.1)(L/6.6)^{3/4}\right)^2} \tag{6}$$

$$\tau[\text{days},\ \text{moderate}] = \frac{200[\text{days pT}^2](E[\text{keV}]/511 + 1)\left((E[\text{keV}]/511 + 1)^2 - 1\right)^{3/4}}{\left((-2.2L + 28.9)(L/6.6)^{3/4}\right)^2} \tag{7}$$

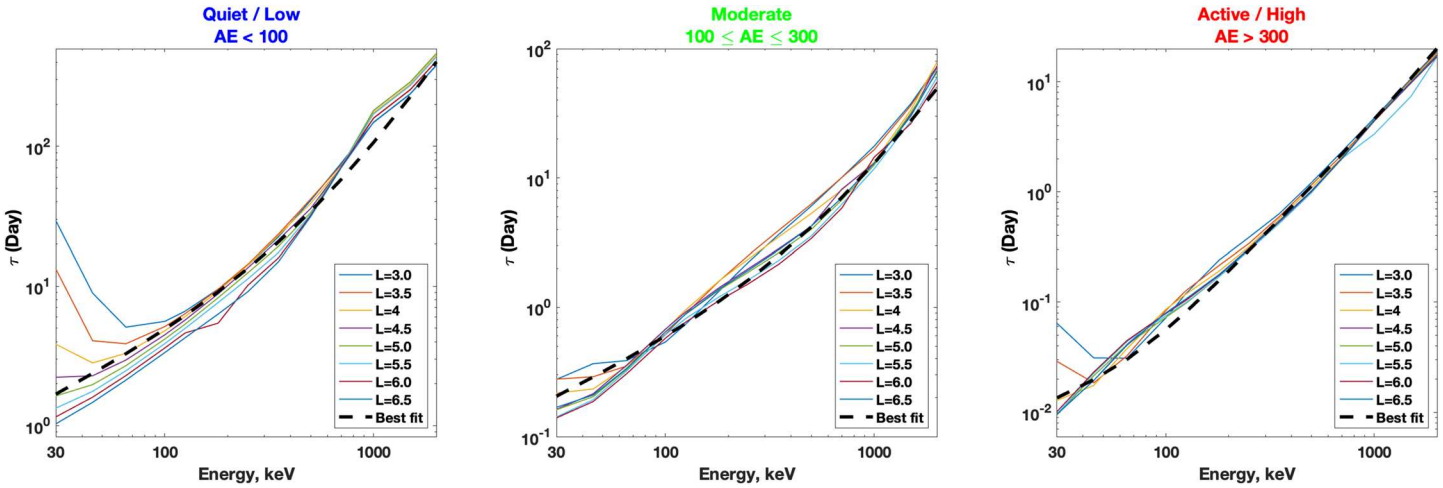

Figure 6. Electron lifetimes as a function of electron energy for quiet (left), moderate (middle), and active (right) geomagnetic conditions. The solid curves indicate numerical model lifetimes at various L-shells. The black dashed curves represent derived best fit analytical lifetime estimates.

$$\tau[\text{days, active}] = \frac{200[\text{days pT}^2](E[\text{keV}]/511+1)\left((E[\text{keV}]/511+1)^2-1\right)^{3/4}}{\left((Bw(30\ keV) * \text{Exp}(-0.1\ \hat{}\ (74/E[\text{keV}]))-6(L-L))(L/6.6)^{3/4}\right)^2} \quad (8)$$

The generalized analytical lifetime formulas (Equations 6–8) can be used to estimate electron lifetimes for different geomagnetic conditions as a function of energy and L-shell in the range of $30 \le E \le 2{,}000$ keV and $3 \le L \le 6.5$, respectively.

Figure 6 shows electron lifetimes as a function of L and electron energy for quiet (left), moderate (middle), and active (right) geomagnetic conditions. The solid curves indicate numerical model lifetimes at $L = 0.5$ intervals for $3 \le L \le 6.5$. The black dashed curves represent the derived best fit analytical lifetime estimates calculated using Equations 6–8 for different geomagnetic conditions. It is clear that the best fit analytical lifetime estimates agree well with full numerical model lifetimes and can be used in general to estimate lifetimes as a function of L and E in the electron energy range of $30 \le E \le 2{,}000$ keV and L-shell in the range of $3 \le L \le 6.5$, although the analytical lifetime energy scaling used in the fits can become inaccurate for E[keV] $< 30(6.6/L)^2$ (for all AE), as noted earlier (Mourenas et al., 2014).

4. Discussion

Many studies have been devoted to calculate electron lifetimes throughout the radiation belts (Albert & Shprits, 2009; Baker et al., 2013; Claudepierre et al., 2020; Fennell et al., 2013; Meredith et al., 2002). Precise calculations of electron lifetimes are crucial for accurately modeling and forecasting the global dynamics of the outer radiation belt and for providing a comprehensive description of electron flux variations over a wide energy range. Predicting the magnitude and duration of potentially hazardous conditions may help satellite operators to switch off nonessential satellite electronic systems to reduce malfunctions and unexpected failures only during the most dangerous periods (Horne, 2007). In this study a synthetic chorus wave model is used to calculate the local pitch angle diffusion coefficients ($D_{\alpha\alpha}$) for electrons over a wide energy range (1 keV to 2 MeV), as a function of geomagnetic activity, L, and MLT. The pitch angle diffusion rates are calculated numerically, assuming that the refractive index of very oblique chorus waves cannot exceed some realistic limits imposed by Landau damping and hot plasma effects (see details in Li, Thorne et al., 2014, and Mourenas et al., 2014, in good agreement with observations; Ma et al., 2017). We then used the full simulation results of MLT-averaged pitch angle diffusion rates to calculate electron lifetimes in a range of L-shells (from $L = 3.0$ to $L = 6.5$) and for a wide range of electron energies (from 1 keV to 2 MeV) as a function of geomagnetic activity.

The importance of electron loss due to resonant chorus wave-particle interactions have been highlighted by various studies (e.g., Albert & Shprits, 2009; Shprits, Elkington et al., 2008; Thorne, 2010). Here the results of

the present model of electron lifetimes are compared with analytical lifetime estimates provided by Mourenas et al. (2014) and with actual lifetime measurements at GEO (Boynton et al., 2014). The present model results (at $L = 6.5$) are in rough agreement with analytical estimates (at $L = 6.5$) over many decades. In particular, the model lifetimes follow approximately the analytical scaling with energy given by Equation 2, except at low energies (<70 keV) and for periods of moderate to high *AE* activity. This is probably partly due to the steep increase of the wave amplitude at low latitudes during disturbed periods, which is not fully taken into account in the analytical estimates. This discrepancy could also be related to the presence of an additional small population of very oblique chorus waves that may reduce lifetimes by a factor 2 as compared with quasi-parallel waves alone for electron energies 30–100 keV (Li, Thorne et al., 2014; Mourenas et al., 2014).

The model lifetimes calculated at $L = 6.5$ have also been compared in Figure 5b with empirical electron lifetimes obtained from 20 years of daily averaged measurements performed by LANL spacecraft at GEO, mainly during low geomagnetic activity. It is worth noting that such GEO measurements actually span a finite range of L-shells. Baker et al. (2019) have notably shown that the geosynchronous spacecraft GOES 15 can span $L \sim 6$ to 8 (more often $L \sim 6.4$–7.5) depending on local time and geomagnetic conditions. Nevertheless, the considered L bin of the chorus wave model is relatively wide, extending from $L = 5$ to $L = 7$, and chorus wave parameters (amplitude and wave normal angle) remain constant within this bin. Since model lifetimes are approximately proportional to $\sim 1/(Bw^2 L^{3/2})$ (see Equation 2), they should vary by less than 15% about their value at $L = 6.5$ inside the range $6 \leq L \leq 7$, limiting potential discrepancies with the measured lifetimes due to differences in L-shells.

The present model results at $L = 6.5$ are in rough agreement with actual lifetimes measured at GEO mainly during weak geomagnetic activity with average $Dst \sim -20$ to -11 nT, often during the late recovery phase of storms (Boynton et al., 2014). In particular, the model lifetimes for nearly quiet periods ($AE < 100$ nT) agree well with the measured lifetimes of moderate energy (20–300 keV) electrons. At higher energies (>300 keV), however, the measured lifetimes become smaller than model lifetimes during low *AE* activity, falling in closer agreement with model lifetimes for moderate activity ($100 < AE < 300$ nT). This behavior is probably partly due to the upper limit of <20 days imposed on measured lifetimes by the method of lifetime determination used by Boynton et al. (2014). Lifetimes larger than ≃18–20 days, corresponding to less than 18–20% reductions in electron flux over a typical flux decay interval (for lifetime evaluation) of 4 days, are indeed very unlikely to be identified by the considered method at energies of 1 MeV or 2 MeV, where electron fluxes are much smaller than at lower energy and a small fluctuation in electron count rates can easily suppress such a weak decay (Boynton et al., 2014). Based on the model lifetimes displayed in Figure 5b, such relatively short <20 days measured 1-MeV electron lifetimes can be obtained only during moderately active periods with $AE > 100$ nT—corresponding to higher average chorus wave amplitudes *Bw* and shorter lifetimes than when $AE < 100$ nT (Li et al., 2011; Shprits et al., 2007). Note that MeV electron fluxes generally reach their peak level at the end of prolonged periods of high substorm activity ($AE > 200$–500 nT, often during early storm recovery), because such electrons need to be accelerated by chorus waves or inward radial diffusion from the bulk of seed <200- to 300-keV electrons directly injected from the plasma sheet (Mourenas et al., 2019; Reeves et al., 2003; Shprits, Elkington et al., 2008; Shprits, Subbotin et al., 2008). Such peaks of MeV electron flux often start to decay a few days later at GEO (Boynton et al., 2014; Mourenas et al., 2019), during periods that can sometimes remain moderately active, with $AE \sim 100$–150 nT. Overall, the present model lifetimes therefore appear in relatively good agreement with observations.

Besides, MeV electron fluxes at GEO often experience rapid dropouts via magnetopause shadowing, caused by sudden impulses of solar wind dynamic pressure or increased southward interplanetary magnetic field (Onsager et al., 2007). However, such rapid dropouts of electron flux by factors >10 over less than 1 day (Boynton et al., 2016; Onsager et al., 2007) are automatically excluded from consideration by the procedure of lifetime selection used by Boynton et al. (2014), limiting the measured lifetimes to slow, wave-driven decay timescales >0.4 days. Although magnetopause shadowing and the related rapid dropouts cannot be invoked as a direct cause of the relatively short lifetimes found by Boynton et al. (2014) at geosynchronous orbit, they could still be the indirect cause of a somewhat slower loss, by leading to a steepening of the negative outward gradient of MeV electron phase space density, thereby helping outward radial diffusion of MeV electrons toward higher L. Indeed, various studies have shown that there is usually a transition from positive to negative gradients of electron phase space density in the outer radiation belt for a magnetic moment $\mu \approx$ 200 MeV/G, corresponding at $L \sim 6.6$ to 0.5–0.2 MeV for pitch angles $\alpha_0 \sim 40$–90° (Turner et al., 2012). By

preferentially scattering high-energy electrons outward (toward lower phase space density), radial diffusion can make the observed lifetimes at a fixed $L = 6.6$ appear smaller above 300 keV. Based on an analytical formulation for the electric field radial diffusion rate due to ultralow frequency (ULF) waves (Ozeke et al., 2014), the corresponding loss timescale of 1-MeV electrons due to outward radial diffusion can be very roughly estimated as ~10 days for $Kp \sim 1$ and a typical phase space density gradient scale length of 1 Earth radius at geosynchronous orbit (Boynton et al., 2014). This effect could therefore explain the shorter mean measured lifetimes <10 days at 1 MeV. Numerical simulations incorporating realistic geomagnetic fields, radial diffusion, chorus-induced loss, and the observed electron phase space density gradients would be necessary to better assess this point.

The general polynomial functions given in Equations 6–8 should be very useful to accurately estimate electron lifetimes needed in radiation belt models, under different geomagnetic conditions and for electrons in the energy range of $30 \leq E \leq 2{,}000$ keV, for L-shells in the range of $3 \leq L \leq 6.5$. Interestingly, Figure 6 shows that the general polynomial fits given in Equations 6–8 are valid over $L = 3.0$–6.5, thanks to the weak variation of model lifetimes with L for a fixed energy. This is due to the relatively weak variation of the lifetimes $\sim 1/L^{3/2}$ for constant $Bw(L)$ (see the analytical lifetime estimate in Equation 2) and to the relatively weak variation of the MLT-averaged Bw with L at a given latitude of cyclotron resonance, below ~30° (e.g., see Figure 1).

5. Conclusion

In this study, we used a synthetic chorus wave model, developed by Agapitov et al. (2018), based on the combined VLF measurements from the Van Allen Probes and Cluster spacecraft to develop a comprehensive parametric model of electron lifetimes in the outer radiation belts. The model takes into account the wave amplitude dependence on geomagnetic latitude, wave normal angle distribution, and variations of wave frequency with latitude. We used the resulting comprehensive synthetic chorus wave model to calculate the local pitch angle diffusion coefficients ($D_{\alpha\alpha}$) for electrons over a wide energy range (1 keV to 2 MeV), as a function of geomagnetic activity level, L, and MLT. We then used the results to estimate electron lifetimes at a range of L-shell (from $L = 3.0$ to $L = 6.5$) as a function of electron energy. The results were compared with previous studies, including analytical results and measured data at GEO. We generalized the analytical formula in Equation 2 by deriving numerically the polynomial function $Bw(L, E)$. The resulting generalized analytical formulas, given by Equations 6–8, can be used to estimate electron lifetimes as a function of L-shell (for $L = 3.0$ to $L = 6.5$), electron energy (from 30 keV to 2 MeV), and different geomagnetic conditions. Overall, the present model lifetimes appear in relatively good agreement with observations, previous studies and analytical results. The results presented in this study are useful for the scientific community. Precise calculations of electron lifetimes are crucial for accurately modeling and forecasting the global dynamics of the outer radiation belt.

Data Availability Statement

The data of the synthetic chorus wave model are available in the form of tables of coefficients in Agapitov et al. (2018), and the original wave data used to develop this model are freely available in the RBSP/EFW database (http://www.space.umn.edu/missions/rbspefw-home-university-of-minnesota/) and in the Cluster Active Archive (https://caa.esac.esa.int/caa/). Wave data from the Van Allen Probes were obtained by the EMFISIS and EFW instruments (Kletzing et al., 2013; Wygant et al., 2013). The Cluster data are gained by STAFF instrument (Cornilleau-Wehrlin et al., 1997), which is part of the WEC wave consortium controlled by DWP (Woolliscroft et al., 1997). Lifetimes measured at Geostationary Earth Orbit are available in Boynton et al. (2014).

Acknowledgments

H. A. and M. A. B. are grateful to the STFC grant (Grant ST/R000697/1). H. A. and J. B. are grateful to NASA H-GCR Award NNX14AI18G and for RBSP-ECT and EMFISIS funding provided by JHU/APL Contracts 967399 and 921647 under NASA's Prime Contract NAS5-01072. The work of O. A. and A. A. was supported by NASA LWS Grant 80NSSC20K021 and NSF Grant 1914670.

References

Agapitov, O. V., Artemyev, A., Krasnoselskikh, V., Khotyaintsev, Y. V., Mourenas, D., Breuillard, H., & Rolland, G. (2013). Statistics of whistler mode waves in the outer radiation belt: Cluster STAFF-SA measurements. *Journal of Geophysical Research: Space Physics*, *118*, 3407–3420. https://doi.org/10.1002/jgra.50312

Agapitov, O. V., Artemyev, A. V., Mourenas, D., Kasahara, Y., & Krasnoselskikh, V. (2014). Inner belt and slot region electron lifetimes and energization rates based on AKEBONO statistics of whistler waves. *Journal of Geophysical Research: Space Physics*, *119*, 2876–2893. https://doi.org/10.1002/2014JA019886

Agapitov, O. V., Artemyev, A. V., Mourenas, D., Mozer, F. S., & Krasnoselskikh, V. (2015). Empirical model of lower band chorus wave distribution in the outer radiation belt. *Journal of Geophysical Research: Space Physics*, *120*, 10,425–10,442. https://doi.org/10.1002/2015JA021829

Agapitov, O. V., Mourenas, D., Artemyev, A. V., & Mozer, F. S. (2016). Exclusion principle for very oblique and parallel lower band chorus waves. *Geophysical Research Letters*, *43*, 11,112–11,120. https://doi.org/10.1002/2016GL071250

Agapitov, O. V., Mourenas, D., Artemyev, A. V., Mozer, F. S., Hospodarsky, G., Bonnell, J., & Krasnoselskikh, V. (2018). Synthetic empirical chorus wave model from combined Van Allen Probes and Cluster statistics. *Journal of Geophysical Research: Space Physics*, *123*, 297–314. https://doi.org/10.1002/2017JA024843

Albert, J., & Shprits, Y. (2009). Estimates of lifetimes against pitch angle diffusion. *Journal of Atmospheric and Solar-Terrestrial Physics*, *71*(16), 1647–1652. Retrieved from http://www.sciencedirect.com/science/article/pii/S1364682608001818 (Toward an Integrated View of Inner Magnetosphere and Radiation Belts) https://doi.org/10.1016/j.jastp.2008.07.004

Artemyev, A., Agapitov, O., Mourenas, D., Krasnoselskikh, V., Shastun, V., & Mozer, F. (2016). Oblique whistler-mode waves in the Earth's inner magnetosphere: Energy distribution, origins, and role in radiation belt dynamics. *Space Science Reviews*, *200*(1), 61–355. https://doi.org/10.1007/s11214-016-0252-5

Artemyev, A. V., Agapitov, O. V., Mourenas, D., Krasnoselskikh, V., & Zelenyi, L. M. (2013). Storm-induced energization of radiation belt electrons: Effect of wave obliquity. *Geophysical Research Letters*, *40*, 4138–4143. https://doi.org/10.1002/grl.50837

Artemyev, A. V., Mourenas, D., Agapitov, O. V., & Krasnoselskikh, V. V. (2015). Relativistic electron scattering by magnetosonic waves: Effects of discrete wave emission and high wave amplitudes. *Physics of Plasmas*, *22*(6), 62,901. https://doi.org/10.1063/1.4922061

Aryan, H., Sibeck, D., Balikhin, M., Agapitov, O., & Kletzing, C. (2016). Observation of chorus waves by the Van Allen Probes: Dependence on solar wind parameters and scale size. *Journal of Geophysical Research: Space Physics*, *121*, 7608–7621. https://doi.org/10.1002/2016JA022775

Aryan, H., Sibeck, D. G., Kang, S. B., Balikhin, M. A., Fok, M. C., Agapitov, O., & Nagai, T. (2017). CIMI simulations with newly developed multiparameter chorus and plasmaspheric hiss wave models. *Journal of Geophysical Research: Space Physics*, *122*, 9344–9357. https://doi.org/10.1002/2017JA024159

Aryan, H., Yearby, K., Balikhin, M., Agapitov, O., Krasnoselskikh, V., & Boynton, R. (2014). Statistical study of chorus wave distributions in the inner magnetosphere using Ae and solar wind parameters. *Journal of Geophysical Research: Space Physics*, *119*, 6131–6144. https://doi.org/10.1002/2014JA019939

Baker, D. N., Kanekal, S. G., Hoxie, V. C., Henderson, M. G., Li, X., Spence, H. E., & Claudepierre, S. G. (2013). A long-lived relativistic electron storage ring embedded in Earth's outer Van Allen Belt. *Science*, *340*, 186–190. https://doi.org/10.1126/science.1233518

Baker, D. N., Zhao, H., Li, X., Kanekal, S. G., Jaynes, A. N., Kress, B. T., & Hoxie, V. (2019). Comparison of Van Allen Probes energetic electron data with corresponding GOES-15 measurements: 2012–2018. *Journal of Geophysical Research: Space Physics*, *124*, 9924–9942. https://doi.org/10.1029/2019JA027331

Bortnik, J., & Meredith, N. P. (2008). The unexpected origin of plasmaspheric hiss from discrete chorus emissions. *Nature*, *452*, 62–66. https://doi.org/10.1038/nature06741

Bortnik, J., & Thorne, R. M. (2007). The dual role of ELF/VLF chorus waves in the acceleration and precipitation of radiation belt electrons. *Journal of Atmospheric and Solar-Terrestrial Physics*, *69*(3), 378–386. https://doi.org/10.1016/j.jastp.2006.05.030

Bortnik, J., Thorne, R. M., & Meredith, N. P. (2007). Modeling the propagation characteristics of chorus using CRRES suprathermal electron fluxes. *Journal of Geophysical Research*, *112*, A08204. https://doi.org/10.1029/2006JA012237

Bortnik, J., Thorne, R. M., Meredith, N. P., & Santolik, O. (2007). Ray tracing of penetrating chorus and its implications for the radiation belts. *Geophysical Research Letters*, *34*, L15109. https://doi.org/10.1029/2007GL030040

Boynton, R. J., Aryan, H., Walker, S. N., Krasnoselskikh, V., & Balikhin, M. A. (2018). The influence of solar wind and geomagnetic indices on lower band chorus emissions in the inner magnetosphere. *Journal of Geophysical Research: Space Physics*, *123*, 9022–9034. https://doi.org/10.1029/2018JA025704

Boynton, R. J., Balikhin, M. A., & Mourenas, D. (2014). Statistical analysis of electron lifetimes at GEO: Comparisons with chorus-driven losses. *Journal of Geophysical Research: Space Physics*, *119*, 6356–6366. https://doi.org/10.1002/2014JA019920

Boynton, R. J., Mourenas, D., & Balikhin, M. A. (2016). Electron flux dropouts at Geostationary Earth Orbit: Occurrences, magnitudes, and main driving factors. *Journal of Geophysical Research: Space Physics*, *121*, 8448–8461. https://doi.org/10.1002/2016JA022916

Breuillard, H., Agapitov, O., Artemyev, A., Kronberg, E. A., Haaland, S. E., Daly, P. W., & Rolland, G. (2015). Field-aligned chorus wave spectral power in Earth's outer radiation belt. *Annales Geophysicae*, *33*(5), 583–597. https://doi.org/10.5194/angeo-33-583-2015

Breuillard, H., Zaliznyak, Y., Krasnoselskikh, V., Agapitov, O., Artemyev, A., & Rolland, G. (2012). Chorus wave-normal statistics in the Earth's radiation belts from ray tracing technique. *Annales Geophysicae*, *30*(8), 1223–1233. https://doi.org/10.5194/angeo-30-1223-2012

Bunch, N. L., Spasojevic, M., Shprits, Y. Y., Gu, X., & Foust, F. (2013). The spectral extent of chorus in the off-equatorial magnetosphere. *Journal of Geophysical Research: Space Physics*, *118*, 1700–1705. https://doi.org/10.1029/2012JA018182

Burtis, W. J., & Helliwell, R. A. (1976). Magnetospheric chorus—Occurrence patterns and normalized frequency. *Planetary Space Science*, *24*, 1007–1024. https://doi.org/10.1016/0032-0633(76)90119-7

Claudepierre, S. G., Ma, Q., Bortnik, J., O'Brien, T. P., Fennell, J. F., & Blake, J. B. (2020). Empirically estimated electron lifetimes in the Earth's radiation belts: Van Allen Probe observations. *Geophysical Research Letters*, *47*, e2019GL086053. https://doi.org/10.1029/2019GL086053

Cornilleau-Wehrlin, N., Chauveau, P., Louis, S., Meyer, A., Nappa, J. M., Perraut, S., & Louarn, P. (1997). The Cluster Spatio-Temporal Analysis of Field Fluctuations (STAFF) experiment. *Space Science Reviews*, *79*, 107–136. https://doi.org/10.1023/A:1004979209565

Fennell, J. F., Kanekal, S., & Roeder, J. L. (2013). Storm responses of radiation belts during Solar Cycle 23: HEO satellite observations, *Dynamics of the Earth's radiation belts and inner magnetosphere* pp. 371–384). Washington, D.C.: American Geophysical Union (AGU). https://doi.org/10.1029/2012GM001356

Horne, R. B. (2007). Plasma astrophysics: Acceleration of killer electrons. *Nature Physics*, *3*, 590–591. https://doi.org/10.1038/nphys703

Horne, R. B., Thorne, R. M., Glauert, S. A., Albert, J. M., Meredith, N. P., & Anderson, R. R. (2005). Timescale for radiation belt electron acceleration by whistler mode chorus waves. *Journal of Geophysical Research*, *110*, A03225. https://doi.org/10.1029/2004JA010811

Huang, C. L., Spence, H. E., Singer, H. J., & Tsyganenko, N. A. (2008). A quantitative assessment of empirical magnetic field models at geosynchronous orbit during magnetic storms. *Journal of Geophysical Research*, *113*, A04208. https://doi.org/10.1029/2007JA012623

Kletzing, C. A., Kurth, W. S., Acuna, M., MacDowall, R. J., Torbert, R. B., Averkamp, T., & Tyler, J. (2013). The Electric and Magnetic Field Instrument Suite and Integrated Science (EMFISIS) on RBSP. *Space Science Reviews*, *179*, 127–181. https://doi.org/10.1007/s11214-013-9993-6

Li, W., Bortnik, J., Thorne, R. M., & Angelopoulos, V. (2011). Global distribution of wave amplitudes and wave normal angles of chorus waves using THEMIS wave observations. *Journal of Geophysical Research*, *116*, 12,205. https://doi.org/10.1029/2011JA017035

Li, W., Ma, Q., Thorne, R. M., Bortnik, J., Zhang, X. J., Li, J., & Goldstein, J. (2016). Radiation belt electron acceleration during the 17 March 2015 geomagnetic storm: Observations and simulations. *Journal of Geophysical Research: Space Physics*, *121*, 5520–5536. https://doi.org/10.1002/2016JA022400

Li, W., Mourenas, D., Artemyev, A. V., Agapitov, O. V., Bortnik, J., Albert, J. M., & Hospodarsky, G. B. (2014). Evidence of stronger pitch angle scattering loss caused by oblique whistler-mode waves as compared with quasi-parallel waves. *Geophysical Research Letters*, *41*, 6063–6070. https://doi.org/10.1002/2014GL061260

Li, W., Thorne, R. M., Ma, Q., Ni, B., Bortnik, J., Baker, D. N., & Claudepierre, S. G. (2014). Radiation belt electron acceleration by chorus waves during the 17 March 2013 storm. *Journal of Geophysical Research: Space Physics*, *119*, 4681–4693. https://doi.org/10.1002/2014JA019945

Lu, G., Tsyganenko, N. A., Lui, A. T. Y., Singer, H. J., Nagai, T., & Kokubun, S. (1999). Modeling of time-evolving magnetic fields during substorms. *Journal of Geophysical Research*, *104*(A6), 12,327–12,337. https://doi.org/10.1029/1999JA900145

Ma, Q., Artemyev, A. V., Mourenas, D., Li, W., Thorne, R. M., Kletzing, C. A., & Wygant, J. (2017). Very oblique whistler mode propagation in the radiation belts: Effects of hot plasma and Landau damping. *Geophysical Research Letters*, *44*, 12,057–12,066. https://doi.org/10.1002/2017GL075892

Ma, Q., Li, W., Thorne, R. M., Nishimura, Y., Zhang, X. J., Reeves, G. D., & Angelopoulos, V. (2016). Simulation of energy-dependent electron diffusion processes in the Earth's outer radiation belt. *Journal of Geophysical Research: Space Physics*, *121*, 4217–4231. https://doi.org/10.1002/2016JA022507

Meredith, N. P., Horne, R. B., & Anderson, R. R. (2001). Substorm dependence of chorus amplitudes: Implications for the acceleration of electrons to relativistic energies. *Journal of Geophysical Research*, *106*, 13,165–13,178. https://doi.org/10.1029/2000JA900156

Meredith, N. P., Horne, R. B., Iles, R. H. A., Thorne, R. M., Heynderickx, D., & Anderson, R. R. (2002). Outer zone relativistic electron acceleration associated with substorm-enhanced whistler mode chorus. *Journal of Geophysical Research*, *107*(A7), 148–227. https://doi.org/10.1029/2001JA900146

Millan, R. M., & Thorne, R. M. (2007). Review of radiation belt relativistic electron losses. *Journal of Atmospheric and Solar-Terrestrial Physics*, *69*, 362–377. https://doi.org/10.1016/j.jastp.2006.06.019

Morley, S. K., Brito, T. V., & Welling, D. T. (2018). Measures of model performance based on the log accuracy ratio. *Space Weather*, *16*, 69–88. https://doi.org/10.1002/2017SW001669

Mourenas, D., Artemyev, A. V., Agapitov, O. V., & Krasnoselskikh, V. (2014). Consequences of geomagnetic activity on energization and loss of radiation belt electrons by oblique chorus waves. *Journal of Geophysical Research: Space Physics*, *119*, 2775–2796. https://doi.org/10.1002/2013JA019674

Mourenas, D., Artemyev, A. V., Ma, Q., Agapitov, O. V., & Li, W. (2016). Fast dropouts of multi-MeV electrons due to combined effects of EMIC and whistler mode waves. *Geophysical Research Letters*, *43*, 4155–4163. https://doi.org/10.1002/2016GL068921

Mourenas, D., Artemyev, A. V., Ripoll, J. F., Agapitov, O. V., & Krasnoselskikh, V. V. (2012). Timescales for electron quasi-linear diffusion by parallel and oblique lower-band chorus waves. *Journal of Geophysical Research*, *117*, A06234. https://doi.org/10.1029/2012JA017717

Mourenas, D., Artemyev, A. V., & Zhang, X. J. (2019). Impact of significant time-integrated geomagnetic activity on 2-MeV electron flux. *Journal of Geophysical Research: Space Physics*, *124*, 4445–4461. https://doi.org/10.1029/2019JA026659

Onsager, T. G., Green, J. C., Reeves, G. D., & Singer, H. J. (2007). Solar wind and magnetospheric conditions leading to the abrupt loss of outer radiation belt electrons. *Journal of Geophysical Research*, *112*, A01202. https://doi.org/10.1029/2006JA011708

Orlova, K., & Shprits, Y. (2014). Model of lifetimes of the outer radiation belt electrons in a realistic magnetic field using realistic chorus wave parameters. *Journal of Geophysical Research: Space Physics*, *119*, 770–780. https://doi.org/10.1002/2013JA019596

Ozeke, L. G., Mann, I. R., Murphy, K. R., Jonathan Rae, I., & Milling, D. K. (2014). Analytic expressions for ULF wave radiation belt radial diffusion coefficients. *Journal of Geophysical Research: Space Physics*, *119*, 1587–1605. https://doi.org/10.1002/2013JA019204

Reeves, G. D., McAdams, K. L., Friedel, R. H. W., & O'Brien, T. P. (2003). Acceleration and loss of relativistic electrons during geomagnetic storms. *Geophysical Research Letters*, *30*(10), 1529. https://doi.org/10.1029/2002GL016513

Santolík, O., Gurnett, D., & Pickett, J. (2004). Multipoint investigation of the source region of storm-time chorus. *Annales Geophysicae*, *22*, 2555–2563. https://doi.org/10.5194/angeo-22-2555-2004

Sazhin, S. S., & Hayakawa, M. (1992). Magnetospheric chorus emissions—A review. *Planetary Space Science*, *40*, 681–697. https://doi.org/10.1016/0032-0633(92)90009-D

Schulz, M., & Lanzerotti, L. J. (1974). Particle diffusion in the radiation belts. *Physics and Chemistry in Space*, *7*, 1974. https://doi.org/10.1007/978-3-642-65675-0

Sheeley, B. W., Moldwin, M. B., Rassoul, H. K., & Anderson, R. R. (2001). An empirical plasmasphere and trough density model: CRRES observations. *Journal of Geophysical Research*, *106*, 25,631–25,642. https://doi.org/10.1029/2000JA000286

Shprits, Y. Y., Chen, L., & Thorne, R. M. (2009). Simulations of pitch angle scattering of relativistic electrons with MLT-dependent diffusion coefficients. *Journal of Geophysical Research*, *114*, A03219. https://doi.org/10.1029/2008JA013695

Shprits, Y. Y., Elkington, S. R., Meredith, N. P., & Subbotin, D. A. (2008). Review of modeling of losses and sources of relativistic electrons in the outer radiation belt I: Radial transport. *Journal of Atmospheric and Solar-Terrestrial Physics*, *70*(14), 1679–1693. Retrieved from http://www.sciencedirect.com/science/article/pii/S1364682608001648 (Dynamic Variability of Earth's Radiation Belts) https://doi.org/10.1016/j.jastp.2008.06.008

Shprits, Y. Y., Meredith, N. P., & Thorne, R. M. (2007). Parameterization of radiation belt electron loss timescales due to interactions with chorus waves. *Geophysical Research Letters*, *34*, L11110. https://doi.org/10.1029/2006GL029050

Shprits, Y. Y., Subbotin, D. A., Meredith, N. P., & Elkington, S. R. (2008). Review of modeling of losses and sources of relativistic electrons in the outer radiation belt II: Local acceleration and loss. *Journal of Atmospheric and Solar-Terrestrial Physics*, *70*, 1694–1713. https://doi.org/10.1016/j.jastp.2008.06.014

Thorne, R. M. (2010). Radiation belt dynamics: The importance of wave-particle interactions. *Geophysical Research Letters*, *37*, 22,107. https://doi.org/10.1029/2010GL044990

Thorne, R. M., Li, W., Ni, B., Ma, Q., Bortnik, J., Chen, L., & Kanekal, S. G. (2013). Rapid local acceleration of relativistic radiation-belt electrons by magnetospheric chorus. *Nature*, *504*, 411–414. https://doi.org/10.1038/nature12889

Tsurutani, B. T., & Smith, E. J. (1974). Postmidnight chorus: A substorm phenomenon. *Journal of Geophysical Research*, *79*, 118–127. https://doi.org/10.1029/JA079i001p00118

Tu, W., Cunningham, G. S., Chen, Y., Morley, S. K., Reeves, G. D., Blake, J. B., & Spence, H. (2014). Event-specific chorus wave and electron seed population models in DREAM3D using the Van Allen Probes. *Geophysical Research Letters*, *41*, 1359–1366. https://doi.org/10.1002/2013GL058819

Turner, D. L., Shprits, Y., Hartinger, M., & Angelopoulos, V. (2012). Explaining sudden losses of outer radiation belt electrons during geomagnetic storms. *Nature Physics*, *8*, 208–212. https://doi.org/10.1038/nphys2185

Woolliscroft, L. J. C., Alleyne, H. S. C., Dunford, C. M., Sumner, A., Thompson, J. A., Walker, S. N., et al. (1997). The digital wave-processing experiment on cluster. *Space Science Reviews*, *79*, 209–231.

Wygant, J. R., Bonnell, J. W., Goetz, K., Ergun, R. E., Mozer, F. S., Bale, S. D., & Tao, J. B. (2013). The Electric Field and Waves Instruments on the Radiation Belt Storm Probes Mission. *Space Science Reviews*, *179*, 183–220. https://doi.org/10.1007/s11214-013-0013-7

Zhang, X. J., Thorne, R., Artemyev, A., Mourenas, D., Angelopoulos, V., Bortnik, J., & Hospodarsky, G. B. (2018). Properties of intense field-aligned lower-band chorus waves: Implications for nonlinear wave-particle interactions. *Journal of Geophysical Research: Space Physics*, *123*, 5379–5393. https://doi.org/10.1029/2018JA025390